Available online at www.sciencedirect.com
SCIENCE DIRECT®
Journal of Colloid and Interface Science 287 (2005) 485–495
JOURNAL OF Colloid and Interface Science
www.elsevier.com/locate/jcis

Preparation and properties of colloidal iron dispersions

K. Butter, K. Kassapidou [1], G.J. Vroege, A.P. Philipse *

Van 't Hoff Laboratory for Physical and Colloid Chemistry, Debye Institute, Utrecht University, Padualaan 8, 3584 CH Utrecht, The Netherlands

Received 30 December 2003; accepted 3 February 2005

Available online 23 March 2005

Abstract

We systematically study the properties of dispersions of iron-based colloids synthesized in a broad size range by thermal decomposition of ironcarbonyl using different stabilizing surfactants. The synthesis results in stable dispersions of monodomain magnetic colloids. Our particles appear to consist of an amorphous $Fe_{0.75}C_{0.25}$ alloy. Sizes of particles coated with modified polyisobutene or oleic acid can be easily controlled in the 2–10 nm range by varying the amounts of reactants. Extensive characterization with various techniques gives particle sizes that agree well with each other. In contrast to dispersions of small particles, which consist of single colloids, dynamic aggregates are present in dispersions of larger particles. On exposure to air, an oxide layer forms on the particle surface, consisting of a disordered Fe(III) oxide.

Keywords: Colloids; Ferrofluids; Magnetic particles; Synthesis and characterization; Size control; Dipolar model system; SAXS; Magnetization measurements; Dynamic susceptibility measurements; (cryo-)TEM

1. Introduction

Ferrofluids (dispersions of magnetic colloids), which have been subject of research for a long time [1,2], are widely used in industrial applications (e.g., in copying machines and printers [3]), but are also important as a model system for dipolar fluids [2,4,5]. In scientific research, magnetite (Fe_3O_4) particles have been investigated extensively, because their synthesis is convenient and well known [6]. However, their polydispersity is large (around 25%) and the variation of particle size is limited (although very recently a different synthesis method of magnetite colloids with very low polydispersity has been described where particle sizes can be controlled better [7]). In contrast, *metallic* magnetic particles can be made quite monodisperse and in various sizes, while having the additional advantage of a larger magnetic moment compared to iron oxides [8]. Metallic iron particles can be synthesized in different ways, for example by chemical vapor deposition [9] or sonolysis [10]. A more convenient and controlled method is the thermal decomposition of metal carbonyl compounds which yields fairly spherical particles under release of carbon monoxide. Colloidal iron particles were synthesized in 1979 by Griffiths et al. [11], who studied iron particles in various solvents using different stabilizing polymers and investigated the oxidation behavior of the particles. Smith and Wychick [12] reported on the kinetics and growth mechanism of the particles. Recently, Pathmamanoharan et al. [13] published preliminary results on the synthesis and characterization of iron particles stabilized with modified polyisobutene (PIB) and oleic acid in decalin. They found that the size of particles grafted with polyisobutene could be controlled well, whereas this was not possible for oleic-acid-coated particles. Because van der Waals and in particular dipolar interactions between particles strongly depend on the particle radius, we expect the microstructure of the fluid (e.g., possible chain formation) and the response to magnetic fields to be sensitive to particle size. To study these size effects properly, monodisperse particles with a large saturation magnetization are needed.

* Corresponding author. Fax: +31 302533870.
E-mail address: a.p.philipse@chem.uu.nl (A.P. Philipse).
[1] Present address: Mininistry of Finance, General Chemical State Laboratory, 16 A. Tsocha Street, 11521 Athens, Greece.

0021-9797/$ – see front matter
doi:10.1016/j.jcis.2005.02.014

Therefore, we present an extensive study on iron dispersions, synthesized by thermal decomposition of ironcarbonyl, in which we systematically varied the radius of particles and studied the effect of size on the physical behavior of magnetic fluids in a broad size range. To stabilize the particles we used two different surfactants, i.e., PIB or oleic acid. The particles were elaborately characterized by a variety of techniques, e.g., magnetization measurements, susceptibility measurements and transmission electron microscopy (TEM), to study the influence of particle size. Throughout these experiments, we especially took care to prevent the dispersions from oxidation by carefully storing and handling all dispersions under dried nitrogen atmosphere. In addition, we studied the oxidation behavior of these systems, by monitoring magnetic properties and size effects on oxidation as a function of time and comparing properties of oxidized and non-oxidized particles. A detailed small-angle X-ray scattering (SAXS) study was included of both oxidized and non-oxidized particles as a function of particle size. The same ferrofluids, of which the synthesis and characterization is described here, are used in (cryo-TEM and dynamic susceptibility) experiments to elucidate their microstructure as a function of particle size [14–17].

2. Experimental

2.1. Materials and methods

Ironpentacarbonyl (Fluka Chemika) was taken from new bottles. Decalin (Merck), oleic acid (Merck, extra pure) and modified polyisobutene (PIB) coded SAP 285, consisting of a mixture of two polymers (Fig. 1) in a mineral base oil (Shell Research Ltd., England), were used as supplied. The modification of polyisobutene was reported elsewhere [18]. According to the supplier, the molecular weight of the PIB is 2400 $g\,mol^{-1}$ and the polyisobutene/polyamine ratio is 2.0–2.5. To protect the iron particles against oxidation, all dispersions were treated and stored under dried nitrogen atmosphere, using schlenks and a glovebox with oxygen pressure lower than 12 ppm (measured by a MBraun MB-OX-SE1 active oxygen probe).

2.2. Synthesis

Dispersions of monodisperse iron particles were synthesized by thermal decomposition of ironpentacarbonyl (a yellow liquid) in decalin in the presence of a stabilizing surfactant (PIB or oleic acid). Decalin is a good solvent for both surfactants and has a high boiling point (∼190 °C), making it very suitable for the synthesis. The mechanically stirred solution was refluxed under nitrogen for 24 h at 170 °C, using an oil bath.

The size of the colloidal particles was tuned by varying the $Fe(CO)_5$/surfactant ratio. The amounts of ironpentacarbonyl, decalin and surfactant used are presented in Table 1. The final dispersions, ordered by increasing radius, are coded A to E (for PIB coated particles) and OA1 to OA3 (for oleic-acid-coated particles). Particles with a large radius (D and E) were prepared by a seed mediated method, adding additional ironpentacarbonyl in portions of approximately 15 ml to a dispersion of smaller particles (C). This method was employed, because earlier experiments where all $Fe(CO)_5$ was added at the start of the synthesis resulted in unstable dispersions. For this seed mediated method the heating was stopped a few hours after the last portion had been added. Oleic-acid-coated particles could not be used

Table 1
Amounts of reactants used for synthesis of iron dispersions

Dispersion code	$Fe(CO)_5$ (ml)	PIB (g)	Oleic acid (g)	Decalin (ml)
A	5	17.5	–	420
B	41	17.5	–	420
C	70	17.5	–	420
D	70 + 56	17.5	–	420
E	70 + 134	17.5	–	420
OA1	7.8	–	5.6	10
OA2	44	–	4	20
OA3	50	–	2.5	60

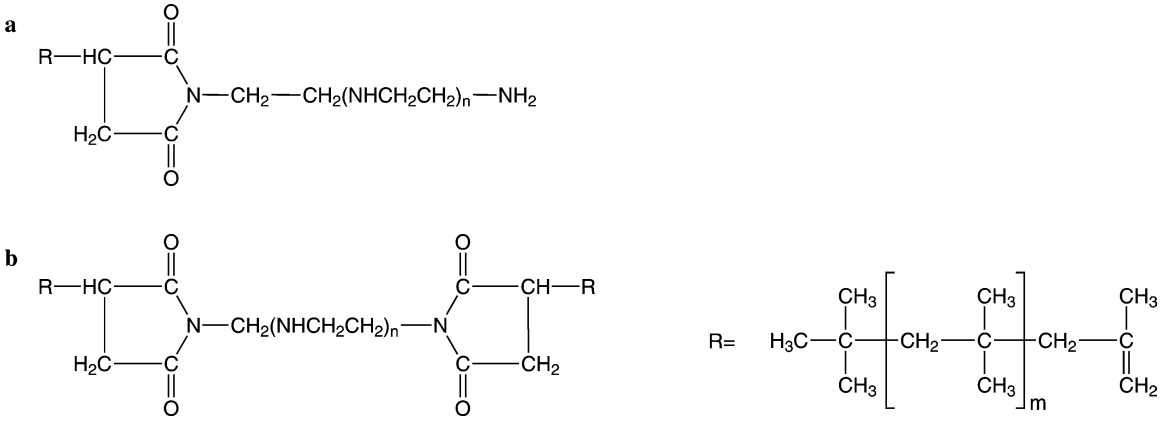

Fig. 1. Structural formula of modified PIB ($m = 41$, $n = 4$). The used substance is 40–50% of a 1:1 mixture of the compounds **a** and **b** in a mineral oil.

Table 2
Size of the iron particles

Code	a_{TEM}[a] (nm)	R_g[b] (nm)	a_G[c] (nm)	a_P[d] (nm)	$R_{g,OX}$[b] (nm)	$a_{P,OX}$[d] (nm)	a_M[e] (nm)	μ_{AGM}[f] ($A\,m^2 \times 10^{19}$)
A	2.1 ± 0.3	1.8 ± 0.05	2.3 ± 0.05	–	2.2 ± 0.04	2.7 ± 0.6	1.3	0.12
B	6.0 ± 0.74	4.1 ± 0.4	5.3 ± 0.5	4.6 ± 0.3	4.6 ± 0.4	5.5 ± 0.6	4.1	4.15
C	6.6 ± 1.1	4.5 ± 0.3	5.9 ± 0.4	5.4 ± 0.3	7.0 ± 1.8	6.4 ± 0.5	5.1	8.38
D	6.9 ± 1.0	6.8 ± 1.8	8.8 ± 2.4	5.4 ± 0.9	8.2 ± 2.9	6.5 ± 0.9	6.0	13.19
E	8.2 ± 1.5	7.4 ± 1.6	9.5 ± 2.1	5.9 ± 0.8	8.7 ± 3.1	7.6 ± 1.5	–	–
OA1	2.2 ± 0.3	1.5 ± 0.03	2.0 ± 0.04	2.1 ± 0.04	2.1 ± 0.04	2.8 ± 0.06	1.2	0.12
OA2	3.2 ± 0.3	2.3 ± 0.05	2.9 ± 0.06	2.9 ± 0.06	2.6 ± 0.05	3.6 ± 0.07	2.4	0.87
OA3	4.3 ± 0.3	3.0 ± 0.06	3.9 ± 0.08	3.8 ± 0.08	–	–	3.3	2.29

Note that the uncertainty in radii obtained from SAXS is due to the measurement method and does not reflect the polydispersity of the sample.
[a] Particle radius measured from TEM micrographs.
[b] Radius of gyration as determined from Guinier curves using Eq. (4).
[c] Guinier radius as determined from radius of gyration using Eq. (5).
[d] Porod radius as determined from maxima in Porod plot.
[e] Magnetic radius determined from magnetization curves via Eq. (3).
[f] Dipole moment $\mu = 4\pi a_M^3 m_s/3$ with bulk value for $Fe_{0.75}C_{0.25}$ ($m_s = 1.49 \times 10^6\ A\,m^{-1}$ [37]).

for this seed mediated synthesis, since this resulted in unstable dispersions.

2.3. Characterization

To check the stability of dispersions, susceptibility measurements at a low frequency (100 Hz) were performed on iron dispersions using a home-built susceptibility meter [15,17] that measures the local susceptibility at a certain height in a sample tube. Details can be found in [16,17]. Transmission electron microscopy (TEM) photographs were made on a Philips CM10H transmission electron microscope from particles on grids coated with a Formvar film. The grids were placed in the vacuum of the sample holder of the microscope within a few minutes after opening of a glovebox under nitrogen atmosphere, in which grids were made by dipping them in a dilute dispersion and leaving them to dry. Particle size distributions were measured using an interactive image analysis program.

Magnetization curves of the dispersions were measured at room temperature on an alternating gradient magnetometer (AGM) Micromag 2900 (Princeton Measurements Corporation) in small airtight glass cups, filled in a glovebox. Measurements were performed at the resonance frequency of the measuring probe (with attached sample), which was in the range 240–290 Hz.

Curves were fitted by the Langevin equation (1), from which M_s was determined:

$$M(H) = M_s\left(\coth\left(\frac{\mu_0\mu H}{kT}\right) - \frac{kT}{\mu_0\mu H}\right). \quad (1)$$

Here, M_s is the saturation magnetization of the sample and the dipole moment of the spheres $\mu = 4\pi a_M^3 m_s/3$ with a_M the magnetic particle radius and m_s the bulk saturation magnetization per volume. $\mu_0 = 4\pi \times 10^{-7}$ T m/A is the magnetic permeability in vacuum. The susceptibility χ_i was determined from the slope of separate curves measured at low magnetic fields ($<1000\ A\,m^{-1}$), since this allowed a more accurate determination of χ_i than via the whole Langevin curve (where the number of measuring points at low fields is small):

$$M(H) = \chi_i H \approx M_s\left(\frac{\mu_0\mu H}{3kT}\right) \quad (\text{for } \mu_0\mu H \ll kT). \quad (2)$$

Assuming a spherical particle shape, particle radii were calculated via Eq. (3), using the bulk value for m_s (see Table 2):

$$a_M^3 = \frac{\chi_i}{M_s}\left(\frac{9kT}{4\pi\mu_0 m_s}\right). \quad (3)$$

The number of particles n in a sample was determined from $M_s = n\mu$. Knowing the sample volume and μ, the particle concentration could be determined. This small volume of samples for AGM measurements (approximately 3 µl) was accurately determined by scaling of χ_i with the susceptibility measured on much larger, known volumes of the same dispersions, using a Kappabridge KLY-3 susceptibility meter (AGICO Corporation, Brno, Czech Republic, operating frequency of 875 Hz). For samples D and E it was known from separate measurements (see [16,17]) that the susceptibility is frequency-dependent in the range of the operating frequencies of the AGM and the Kappabridge susceptibility meter, so the volume could not be determined by calibration with the Kappabridge. In these cases, the value for n is not given here. The concentration of iron in all dispersions was determined by elemental analysis of a known amount of dispersion from which the iron particles were extracted (by flocculating them with pentanol) and dried. From both n and the iron concentration the volume fraction of iron cores was estimated, using the particle density (see Table 3) and the particle TEM radius (Table 2). The maximal theoretical volume fraction (Table 3) was calculated from the particle mass density and the amount of ironcarbonyl used in the synthesis (Table 1).

Table 3
Concentration of iron particles

Code	Fe amount (mass fraction)[a]	Conc.$_{AGM}$ (particles/l)[b]	ϕ_{EA}[c]	ϕ_{AGM}[d]	$\phi_{theoretical}$[e]
A	0.004	1.7×10^{19}	0.00059	0.00066	0.00070
B	0.038	8.0×10^{18}	0.0049	0.0072	0.0057
C	0.061	8.2×10^{18}	0.0079	0.0099	0.0098
D	0.108	–	0.015	–	0.018
E	0.219	–	0.027	–	0.029
OA1	0.0824	3.1×10^{20}	0.0056	0.014	0.046
OA2	0.0587	1.0×10^{21}	0.064	0.14	0.13
OA3	0.257	1.4×10^{20}	0.038	0.047	0.049

[a] Amount of iron in dispersion from elemental analysis (g Fe/g dispersion).
[b] Particle concentration determined from AGM measurements using the values for M_s, μ and sample volume.
[c] Iron volume fractions using results from elemental analysis and a density for $Fe_{0.75}C_{0.25}$ of 7.58 g/cm^3 [37].
[d] Iron volume fractions using results from column 3 and the TEM radius.
[e] Maximum theoretical iron volume fraction using the amount of $Fe(CO)_5$ used in the synthesis and a density for $Fe_{0.75}C_{0.25}$ of 7.58 g/cm^3 [37].

2.4. SAXS measurements

Small-angle X-ray scattering experiments were performed at the hard branch of the DUBBLE (Dutch–Belgian beamline) at the European Synchrotron Radiation Facility (ESRF) in Grenoble, France. Dispersions of PIB-coated and oleic-acid-coated particles were measured at different q ranges of 0.05–1.35 and 0.04–3 nm^{-1}, respectively. The measured two-dimensional diffraction patterns were corrected for transmission, background radiation and detector response. All measured intensities are in arbitrary units and only have relative relevance. The measurements were performed on dilute dispersions A to E and OA1 to OA3 before and after oxidation. In this paper, the dilution factor is given in brackets directly behind the dispersion code, e.g., C(5) is dispersion C, diluted five times. Stock dispersion C was also measured. The concentrations of the non-diluted samples are given in Table 3. The suspensions were sealed in airtight glass capillaries. The radius of gyration R_g was obtained from the scattering at low q values ($q < 2/R_g$) [19,20],

$$I(q) = I(q=0)\exp\left(-q^2 R_g^2/3\right), \tag{4}$$

with q the momentum transfer vector. Plotting $\ln I(q)$ versus q^2 (Guinier plot) for small q should yield a straight line with slope $R_g^2/3$. Assuming homogeneous spheres, the radius of gyration is related to the sphere radius a by

$$R_g^2 = 3a^2/5. \tag{5}$$

In a so-called Porod plot the complete scattering curve is used. $I(q)$ multiplied by q^4 is plotted versus q on a linear scale. The positions of the first maximum (q_{max}) and the first minimum (q_{min}) in this plot yield the particle radius a_P (here indicated as Porod radius) for homogeneous spheres via [21]

$$a_P = 2.74/q_{max} = 4.49/q_{min}. \tag{6}$$

Note that a_P is not equal to the radius obtained from the specific surface of the phase boundary using the Porod plot at high q values [19]. The radius obtained from the Guinier plot and from the Porod plot should be the same for homogeneous monodisperse spheres. For polydisperse systems, the particle radius as determined from both the Guinier plot (which equals $(\langle r^8\rangle/\langle r^6\rangle)^{1/2}$ [20,22] for narrow size distributions) and the Porod plot ($= \langle r^7\rangle/\langle r^6\rangle$ [23]) should be corrected for polydispersity to obtain the average particle radius number [20,22]. Other factors, e.g., aggregation of particles, could result in a difference between the Porod and Guinier radius; the Guinier plot is known to be influenced dramatically by clustering, which causes the scattering at low q values to increase [19], while the Porod radius is not influenced significantly [19].

To obtain the experimental static structure factor over the measured q range for dispersions at a given volume fraction, the scattered intensities were divided by those of the lowest volume fraction C(5) and scaled to the concentration. Here, it was assumed that no interparticle interaction is present in the dilute dispersion. The peak in the static structure factor for hard spheres corresponds roughly to the distance d_c of nearest approach between particles, given by Bragg's law [19],

$$d_c q_{max} = 2\pi, \tag{7}$$

where q_{max} is the q value at the maximum intensity and d_c is the center-to-center distance at nearest approach. For a dispersion of monodisperse hard spheres, a fairly accurate description of $S(q)$ was obtained from the Percus–Yevick integral equation [24] for the radial distribution function $g(r)$ which could be solved analytically [25,26]. For this paper, calculations of structure factors for *polydisperse* hard spheres were performed using a computer program by van Beurten and Vrij [27] based on a closed expression for the scattering intensity of any number p of hard sphere components as derived by Vrij [28] using the Baxter [29] solution of the Percus–Yevick equation.

2.5. Oxidation behavior

To study the oxidation behavior of iron particles, the thickness of a layer with decreased contrast visible on TEM micrographs made at different moments after exposing a TEM grid with particles from dispersion C to air, was determined by an interactive image analysis program. In addition, magnetic susceptibility measurements were performed with a Kappabridge KLY-3 susceptibility meter (Agico) at 875 Hz at several moments after exposing containers, filled with equal amounts of dispersion in a glovebox, to air. Because decalin has a very low vapor pressure, a correction for evaporation was not performed.

To characterize the oxide formed on the particles transmission infrared spectroscopy measurements were performed on a Perkin Elmer 2000 infrared spectrophotometer (resolution 4 cm^{-1}). Spectra were measured by averaging

100 scans of a measuring cell, on which a droplet was spread of a dispersion that had been exposed to air for a few weeks. X-ray diffraction spectroscopy was performed with a Nonius Powder diffractometer on samples which were dried in air. The wavelength of the radiation was 1.789 Å.

3. Results

3.1. Synthesis

Approximately 30 min after we started to heat the mixture, the yellow ironpentacarbonyl solution turned either brown (dispersion A) or black (for larger particles), due to the formation of iron. Dispersions B to E, OA2 and OA3 could be manipulated by the field gradient of a small permanent magnet. Going from system A to E, the dispersion viscosity appeared to increase as judged by the slower response to tilting of the vessel. Dispersions kept under nitrogen were stable for years (i.e., no flocs or sediment were observed). However, a few days after having been exposed to air, dispersions became unstable and the systems D and E formed a spacefilling gel, which could be turned upside down without flowing. This gel was also formed in closed containers, which had been exposed to air for a short time. When the gel was diluted, an unstable dispersion was formed, which sedimented within a few hours. The oxidation behavior of the dispersions is further discussed in Sections 3.4 and 4.4.

3.2. Characterization

For all dispersions, the susceptibility was independent of height in the sample tube, which indicates that our dispersions are stable and do not phase separate.

Fig. 2 shows typical TEM micrographs of all dispersions. The stabilizing polymer layer around the particles is invisible on these pictures. The particles do not touch each other, which is an important indication that they are not aggregated. The size of the iron cores and their standard deviation (7–18%), measured from the micrographs, is given in Table 2. It appears that oleic-acid-coated particles are less polydisperse and have a more spherical shape than PIB-coated particles, which sometimes show irregular surfaces (most clearly for dispersion C, Fig. 10a).

Magnetization curves (Fig. 3) of dispersions A to D did not show any hysteresis and could be properly fitted with the Langevin equation (1), indicating that the particles are monodomain and superparamagnetic. The magnetic particle radii and particle concentration determined from the measurements are given in Tables 2 and 3, respectively. For dispersion E, the particle size could not be calculated from the magnetization curve because of its hysteresis. The maximum theoretical volume fractions and the volume fractions determined from elemental analysis are also given in Table 3.

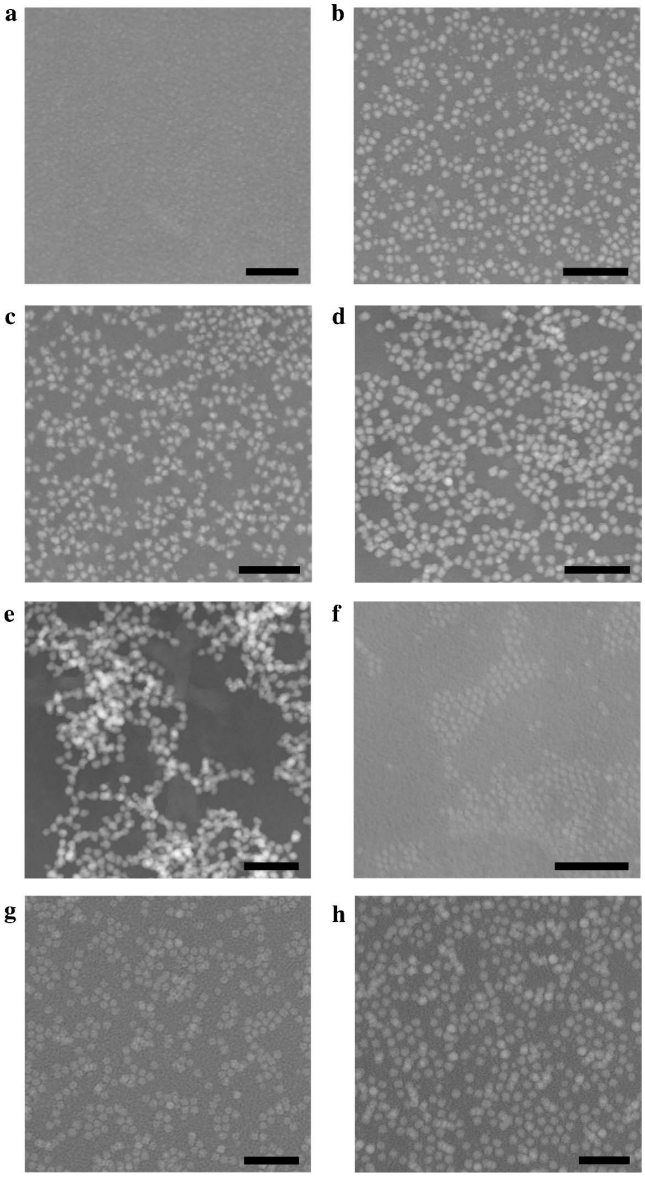

Fig. 2. TEM pictures of dispersions (a) A, (b) B, (c) C, (d) D, (e) E, (f) OA1, (g) OA2, and (h) OA3. Scale bars are 50 nm (a, f–h) or 100 nm (b–e). (a) and (f) illustrate that the sizes of the smallest particles are at the limit of the microscope resolution. However, the original micrographs are sufficiently clear to measure their size.

3.3. SAXS measurements

As an illustrative example, Fig. 4 presents the scattered intensities from dispersion C for three different concentrations, divided by their concentration. Due to the large difference in electron density between the iron core of the colloidal particles and the solvent, contrary to the very small contrast of the grafted polymer layer, the scattering from the latter can be neglected. It can be observed that the two lower concentrations do not exhibit any interparticle structure, while the highest concentration shows clearly structure at low q.

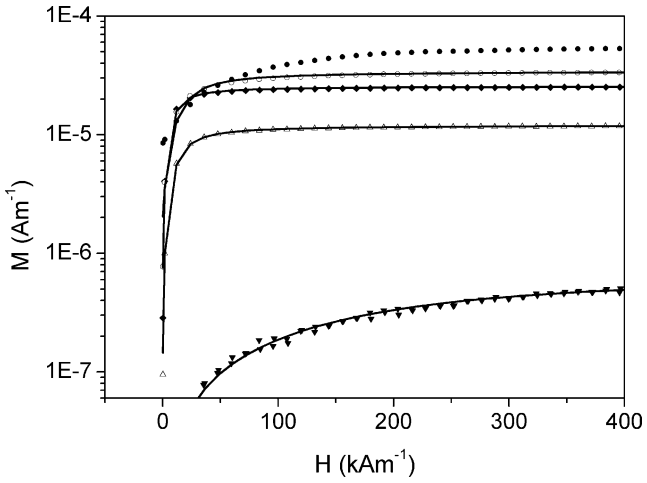

Fig. 3. Magnetization curves of dispersion A (▼), B (△), C (◆), D (○), and E (●). The solid lines are Langevin fits. Dispersion E could not be fitted properly due to hysteresis at low fields. Values for χ_i were determined from separate curves measured at low magnetic fields (<1000 A m^{-1}).

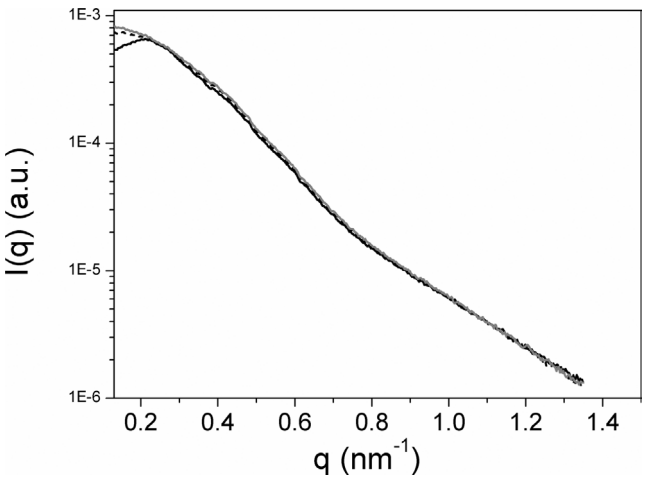

Fig. 4. Scattered intensities normalized to concentration for samples C (black solid line), C(2) (black dashed), and C(5) (gray solid line).

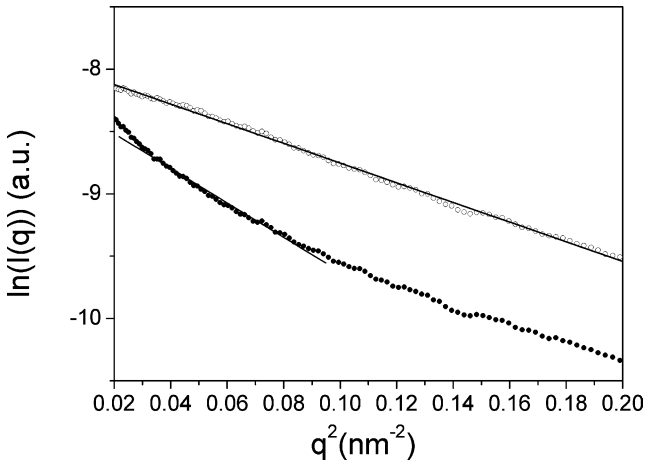

Fig. 5. Guinier plot [$\ln I(q)$ vs q^2] of dispersion C(5) (○) and D(10) (●). The curve of D(10) shows a steep upturn at low q, indicating aggregation.

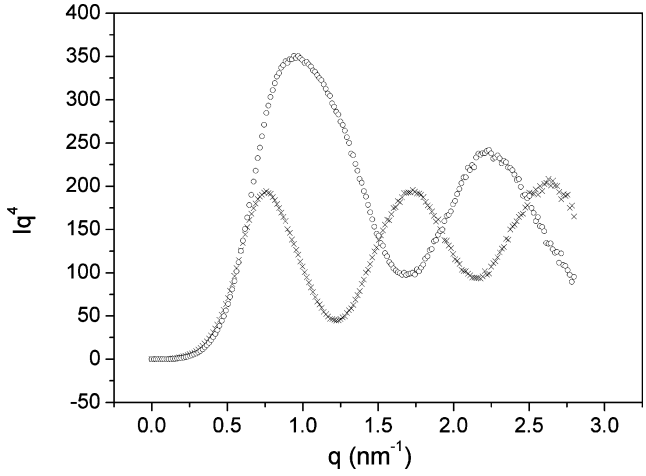

Fig. 6. Porod plot [$I(q)q^4$ vs q] for oxidized (×) and non-oxidized OA2(2) (○) samples. The increasing intensity with q for the oxidized sample probably is an artifact arising from problematic background correction.

Fig. 5 presents the Guinier plots of dispersions C(5) and D(10). The lines are the best least-square fit to the data. From the slope of this line the particle radius was calculated according to Eqs. (4) and (5). The radii of gyration and Guinier radii for all dispersions are given in Table 2. Since not all Guinier curves were perfectly linear, especially not for the larger particles (D and E), a considerable spread in the Guinier radii was found, depending on the exact part of the curve used for the Guinier fit. For particles B, although the Guinier curve was straight, resulting in a small error in the fit, a larger difference was found in the Guinier radii obtained in different measuring sessions, so that the final uncertainty in the value is significant. For the oxidized systems and dispersions D and E, the Guinier plots showed a steep upturn at low q (see Fig. 5 for dispersion D), indicating aggregation. In these cases, the determination of the radius of gyration was even less accurate. The estimated uncertainty in the radii is indicated in Table 2. Note that this uncertainty is due to the measurement method and not to polydispersity, the predominant cause of the spread in TEM radii.

Fig. 6 shows an example of the Porod plot of particles OA2(2) for the oxidized and the non-oxidized sample. The positions of the minima and the maxima in the Porod plots were determined by differentiating the curves and equating the first derivative to zero. The particle radii obtained from the first maximum of the Porod plots (further indicated as Porod radii) for both the non-oxidized and oxidized particles of all dispersions are given in Table 2. In some cases the peaks were rather broad, resulting in a considerable uncertainty in the radii, which is also indicated in the table.

Fig. 7 shows the experimental static structure factor for non-oxidized particles C (samples C(2) and C, data from other samples not shown). From the position of the maximum the closest particle distance could be estimated using Eq. (7). As mentioned above, the grafted polymer chains are virtually matched. However, the closest interparticle distance is determined by the diameter of the whole core–shell

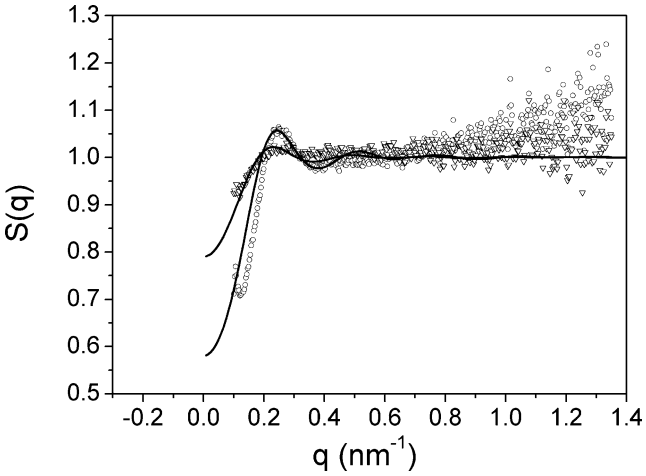

Fig. 7. Static structure factor of particles C (non-oxidized) in decalin versus q for two different volume fractions (samples C (○) and C(2) (▽)). The scattered intensities have been divided by the scattered intensity of the sample with the lowest volume fraction (C(5)). Probably due to the use of cylindrical capillaries (where the path length depends on the exact position of the capillary with respect to the beam) or inaccuracies in the concentrations, the structure factors had to be corrected to achieve a value of 1 at higher q. The solid lines are the structure factors for hard spheres with a lognormal size distribution. The parameters used are a core radius a_{core} of 6.6 nm with standard deviation $\sigma = 0.35$ and a surfactant layer thickness (without contrast) of 5.4 nm. The volume fractions of the calculated curves are 0.07 and 0.03 for C and C(2), respectively.

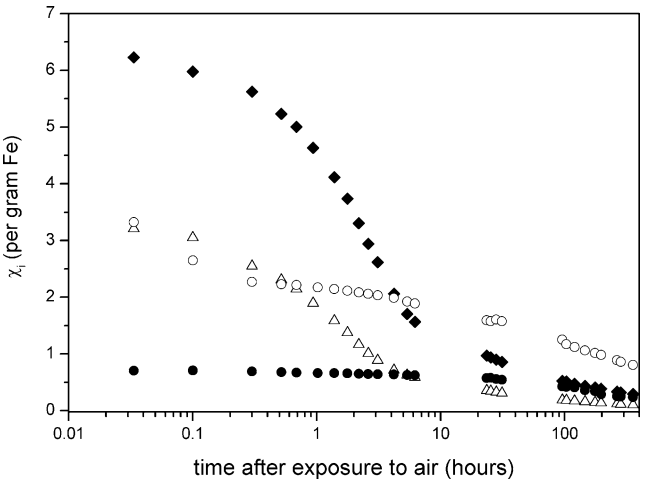

Fig. 8. Decreasing susceptibility of dispersions B (△), C (◆), D (○), and E (●) in time during exposure to air.

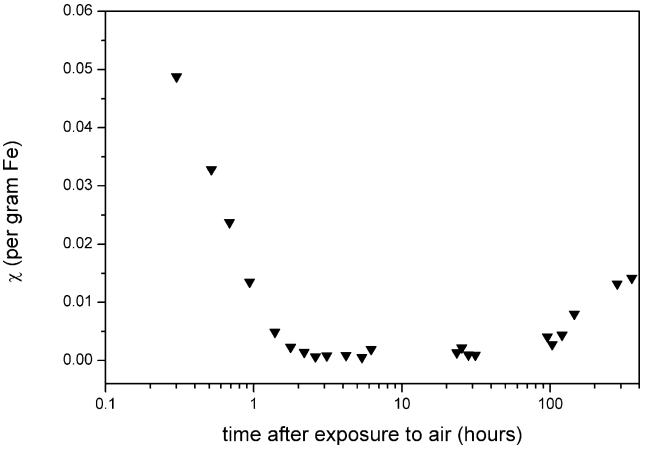

Fig. 9. Decreasing susceptibility of dispersion A in time during exposure to air.

particle. Therefore, the thickness of the polymer layer could be estimated from the position of the maximum in the structure factor as approximately 6 nm.

The curves could reasonably well be described with the structure factor for polydisperse hard spheres (with average core radius $\langle a_{\text{core}} \rangle$ of 6.6 nm) with lognormal size distribution $P(a_{\text{core}})$ with standard deviation $\sigma = 0.35$ and a surfactant layer (without scattering contrast) of 5.4 nm.

3.4. Oxidation measurements

The decrease of susceptibility in time per gram iron after exposing the dispersions to air can be seen in Figs. 8 and 9. In the first few hours the susceptibility decreased fast, after which it slowed down, though a decrease was still noticeable even after 700 h. The curve for dispersion A is inaccurate because of the low positive values of the susceptibility (of the order of the negative susceptibility of the vessel), but the susceptibility was decreasing very fast. As expected, the susceptibility was decreasing more slowly for larger particles, because their surface/volume ratio is smaller. While after 100 h the susceptibility of dispersions A, B and C had decreased to below 10% of the starting values, dispersions D and E still had a susceptibility of respectively 35% and 60% of the original value.

On TEM micrographs of oxidized particles a shell with a lower contrast could be observed around the iron cores, indicating an oxide layer at the surface of the particles (Fig. 10). Formation of an oxide surface layer was also found from small angle neutron scattering measurements that we performed on oleic-acid-coated iron particles synthesized via the same method [17,30]. It seems that this passivating oxide layer considerably slowed down the oxidation. TEM micrographs of dispersion C, from which the grids were made under nitrogen atmosphere, showed that an oxidized layer of 2.4 nm developed in approximately 80 min when exposing the grid to air, while the radius of the particle had increased from 6.7 to 7.1 nm in this period. However, a non-oxidized iron core was visible even after a period of months, so the particles were not completely oxidized. From the dimensions of the iron core before and after oxidation, and the thickness of the oxidized layer after oxidation it was estimated that the volume of a certain amount of iron is becoming 1.3 times as large upon oxidation. Note that in this number, the error is rather large; an estimated error of 10% in the sizes measured with TEM results in a standard deviation of 65%.

The infrared spectra of oxidized particles did show several peaks, none of which were characteristic for bulk mag-

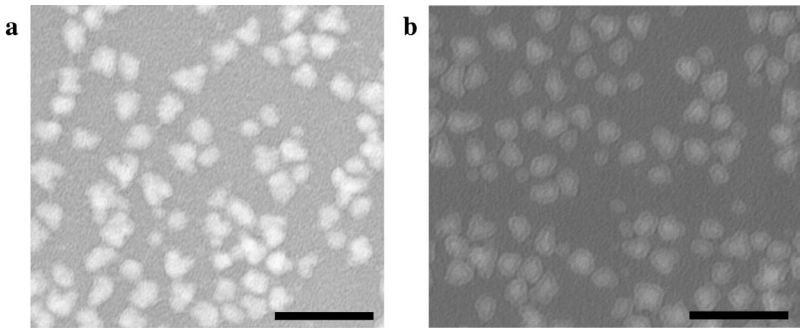

Fig. 10. TEM pictures of dispersion C (a) without exposure to air and (b) after exposure of the grid to air for three weeks. Scale bars correspond to 50 nm.

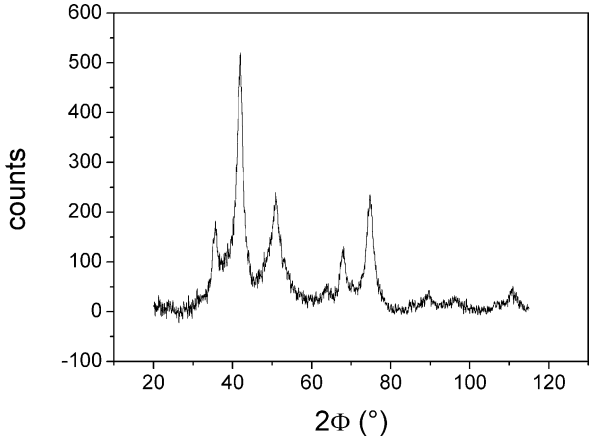

Fig. 11. XRD spectrum of dispersion C after exposure to air for a few weeks.

Table 4
XRD peaks for magnetite (Fe_3O_4) [32]

d (Å)	2θ	Relative intensity	$h\ k\ l$
2.967	35.09	30	2 2 0
2.532	41.38	100	3 1 1
2.0993	50.44	20	4 0 0
1.6158	67.23	30	5 1 1
1.4845	74.11	40	4 4 0

netite or hematite, however. Oleic-acid-coated particles exhibited peaks at 2800–3000 cm^{-1} and 1400–1500 cm^{-1}, corresponding to alkane stretch and bending vibrations from oleic acid [31]. The peaks in the XRD spectrum of oxidized particles C (Fig. 11) correspond well with Ref. [32] of magnetite (Table 4), although peaks are rather broad.

4. Discussion

For completeness, we will include in this section some results from Mössbauer spectroscopy measurements published elsewhere [33], performed on the same dispersions A, C and E that are described here (corresponding to the samples in their Figs. 1d, 1b and 1a, respectively; note that the particle radius used in Ref. [33] is a preliminary estimate and is different from the real particle size as in Table 2 of this paper).

4.1. Synthesis

All dispersions in this study are stable, as judged by visual observations and susceptibility measurements (see [15,17]). This indicates that PIB and oleic acid are adsorbed on the iron surface, in accordance with earlier results for similar systems [34]. Large particles can be grown out of smaller PIB-coated particles without adding extra surfactant. Since dispersions D and E are still stabilized by the PIB surfactant layer, PIB molecules probably can move parallel to the surface of particles allowing newly formed iron to precipitate on the iron core. However, the surfactant density on particles D and E presumably will be lower than for dispersions synthesized without seed particles.

4.2. Characterization

Particle radii measured with various techniques (Table 2) correspond well with each other and show that the particle size increases with increasing $Fe(CO)_5$/surfactant ratio used for their synthesis. In contrast to what was found by Pathmamanoharan et al. [13], not only sizes of particles coated with PIB but also oleic-acid-coated particle sizes could be controlled well. The reason presumably is that the authors of Ref. [13] did not take special care of excluding oxygen before measuring particle sizes with TEM. As discussed in Sections 3.4 and 4.4, particle sizes increase considerably upon oxidation.

In general, the TEM radii for our dispersions are somewhat larger than the particle sizes from SAXS, certainly when the latter ones are corrected for polydispersity. This may be due to a slight oxidation (not yet visible by electron microscopy) of particles on the TEM grids just before positioning them in the microscope. In addition, TEM radii for such small particles presumably contain a relatively large uncertainty, since we found that particle radii measured on various electron microscopes differed up to 20%. For most systems, the radii determined from the magnetization measurements are significantly smaller than the TEM/SAXS radii. The difference can be ascribed to demagnetization of the near-surface region of the magnetic material, a general observation in ferrofluids [2]. Note that magnetic radii were calculated using the bulk value of $Fe_{0.75}C_{0.25}$ for m_s, which

may not be completely correct. This point is further discussed in [17,30].

Volume fractions of iron (determined via different methods, see Table 3) are in reasonable agreement with each other. For PIB-coated particles, the iron concentration is almost equal to the theoretical value, as calculated from the used amounts of reactants. This agrees with the absence of free $Fe(CO)_5$ in the dispersions, as was also found from Mössbauer spectroscopy on PIB-coated samples [35]. However, for oleic-acid-coated particles OA1 and OA2, the experimental iron volume fractions are much lower than the maximum theoretical value. Presumably, in this case part of the ironpentacarbonyl was not converted, as was also found by Mössbauer spectroscopy of a separate sample of oleic-acid-coated particles. In some cases (B, OA2), the values for ϕ_{AGM} are somewhat larger than the maximum theoretical values. This is ascribed to the fact that for calculation of ϕ_{AGM} the TEM radius was used, which may be somewhat too large.

From Mössbauer spectra of dispersions C and E (stored and measured under nitrogen atmosphere) it appeared that a significant amount of carbon is present in the particles, which were determined to consist of $Fe_{0.75}C_{0.25}$ [33]. Presumably, the carbon originates from $Fe(CO)_5$ and is incorporated in the particles during synthesis. The same composition was also found by other authors [36] for oleic-acid-coated iron particles synthesized via the same method we used. Therefore, it is a plausible assumption that all iron dispersions described in this paper consist of $Fe_{0.75}C_{0.25}$. In addition, the spectrum of particles C shows a small contribution of a Fe(III) oxide [33]. This could be explained by the presence of a small amount of oxygen during drying of the sample. The oxidic contribution is absent in the spectrum of particles E (measured as frozen liquid). To protect the smallest particles (A) against oxidation is difficult; Mössbauer spectroscopy [33] revealed that despite careful precautions to exclude oxygen, particles A are almost completely oxidized. Similar results were found from SAXS measurements (increase of particle size in time due to oxidation). This means that results on particle radii measurements of dispersion A are not very reliable. For the dispersions of larger PIB-coated particles (B–E), serious unintentional oxidation appeared to be absent, although a slight oxidation (maximum of 15% decrease in susceptibility over 4 years) was measured. All measurements on our oleic-acid-coated particles were performed within 5 months after their synthesis, so that substantial oxidation during storage was avoided.

On TEM pictures one can see that the mutual positions of the particles depend on their size. Small particles are randomly distributed, while larger particles (E) show linear structures, but particles do not touch each other. Although these pictures are made from dried grids, which in principle do not provide information on particle arrangement in the fluid state, cryo-TEM on the same samples confirm the presence of anisotropic aggregates in vitrified thin films of samples D and E [14,15,17]. These results are supported by the hysteresis present in the magnetization curve of dispersion E. Because the Brownian relaxation time for single particles of this size is approximately 3×10^{-5} s, much smaller than the scanning speed of the AGM of 200 ms per measuring point, hysteresis behavior is not expected for a system of separate particles. Therefore, much larger, slowly relaxing structures, must be present in the dispersion. The presence of larger aggregates is consistent with the increasing viscosity with particle size, which for single spherical particles is not expected to increase much for low volume fractions. Larger dynamic structures in both dispersions D and E are also found from frequency-resolved susceptibility measurements described in [16,17]. Probably, the magnetization curve of dispersion D does not show hysteresis, because the structures present here are much smaller [14,15,17] and therefore have shorter relaxation times than in dispersion E.

4.3. SAXS measurements

The data from SAXS show that the Porod radii generally are somewhat smaller than the Guinier radii but are in reasonable agreement for dispersions of relatively small particles (OA1–OA3). However, the discrepancy between the Porod and Guinier radius for dispersions D and E is rather large and presumably is the result of aggregation. The presence of aggregates was also found in the Guinier plots of these dispersions, showing a steep upturn at low q and preventing an accurate determination of the radius of gyration of single particles. Aggregate formation is not expected to influence the Porod radius significantly, since in the aggregates the iron cores are not expected to fuse. The discrepancy between the Porod and Guinier radii cannot be ascribed to polydispersity, since both values are influenced almost equally by a size distribution of the particles (see Section 2.4). For dispersions B and C, where no signs of aggregation were detected, the difference between the Guinier and Porod radius probably is the result of inhomogeneity of the particles (which consist of an amorphous iron–carbon alloy), causing the extrema in the Porod plot to shift to smaller q values.

The radii of gyration of oxidized particles are about 1.2–1.5 times the radii of gyration of the non-oxidized particles, consistent with the other indications of particle volume increase upon oxidation. The same effect is found for the Porod radius, which is found to become up to 1.4 times larger upon oxidation. However, it is unlikely that the whole particle is transformed into iron oxide, as was also found from TEM, AGM and Mössbauer measurements (Sections 3.4 and 4.4). Apparently, there is a layer of iron oxide covering a core of $Fe_{0.75}C_{0.25}$. Due to this partial oxidation, the modeling of the oxidized particles as spheres with a uniform electron density is not completely correct. However, since the exact thickness and electron density of the iron oxide layer is not known, no better approximation for the Porod radius could be made. On the other hand, the Guinier radii determined for the oxidized particles deviate signifi-

cantly from the Porod radii. Moreover, the Guinier plot of most of the oxidized particles shows a steep upturn at very low q (data not shown), signifying that these particles also tend to aggregate. Therefore, the Guinier radii of these particles could not be fitted properly and they certainly include contribution of the larger aggregates.

From the interparticle spacing derived from the positions of the maxima in the static structure factors of dispersions C (see Fig. 7), a thickness of a polymer layer of about 5–6 nm was determined. These experimental structure factors could be reasonably well described by a structure factor for polydisperse hard spheres. The parameters for average particle radius (6.6 nm) and polydispersity (0.35 nm) are in reasonable agreement with results from other measurements (see Table 2), although the polydispersity is lower than found with TEM. Also the values for the volume fractions used in the theoretical structure factors describing our data (of particles including the surfactant shell of about 6 nm) are consistent with what is expected from the volume fraction of the iron cores (see Table 3).

4.4. Oxidation behavior

TEM micrographs show that upon oxidation of the particles an oxide layer is formed at their surface. This is consistent with the decrease of oxidation rate with time; a passivating oxide layer slows down the oxidation process. On oxidation of particles C and E the Mössbauer spectra showed a contribution of a disordered Fe(III) oxidic species [33]. In agreement with TEM pictures and susceptibility measurements, Mössbauer spectroscopy of particles E showed that they only oxidize partly [33].

Upon oxidation, dispersions become unstable within a few days and particles sediment, probably because particle surface area increases (and surfactant density decreases) due to oxidation. Dispersions of larger particles (D and E) even form a space-filling gel, possibly because of the higher volume fractions involved. From the values of the saturation magnetization before and after oxidation and the thickness of the oxidized layer from TEM micrographs, never exceeding 3 nm (after a few months of exposure to air), it can be argued that the formed oxide is not pure magnetite or maghemite, because the magnetic moment has decreased too much for that: the saturation magnetization m_s per volume for $Fe_{0.75}C_{0.25}$ is estimated to be 1.49×10^6 A m^{-1} (using a density of 7.58 g/ml (Table 4 in [37]) and $m_s = 1.59\mu_B$/Fe atom [37]), while for magnetite and maghemite this is approximately 0.48×10^6 A m^{-1} [8]. Also from the infrared spectra it is clear that our oxidized particles do not consist of pure hematite or magnetite. However, XRD spectra show peaks that correspond to magnetite, although broader than for the perfectly crystalline oxide.

Possibly the structure of the oxide is an amorphous nonmagnetic iron oxide, which does not contribute to the magnetic moment of the particle. The volume increase with a factor of 1.3 upon oxidation is somewhat lower than the value of 2.1 that is expected from bulk densities when metallic iron is transformed into magnetite, maghemite or hematite. However, since measurements of such thin oxide layers on TEM micrographs are not very accurate, the value of 1.3 seems a reasonable one.

From the susceptibility measurements as a function of time (Fig. 8), the low susceptibility of dispersions D and E in comparison with other samples seems remarkable, since the initial susceptibility scales with μM_s (see Eq. (2)), as is indeed experimentally found for dispersions B and C (at $t = 0$). Frequency-dependent susceptibility measurements [16,17] of dispersion E show a decrease of the susceptibility with frequency, starting from 1 Hz. This can explain the low susceptibility at 875 Hz, the measuring frequency of the Kappabridge susceptibility meter. The same argument holds for dispersion D, but here the effect is less strong because the aggregates are smaller.

5. Conclusions

We synthesized stable dispersions of superparamagnetic monodomain iron-based particles in a broad size range with low polydispersity using different surfactants. Particle sizes can be controlled by varying the $Fe(CO)_5$/surfactant ratio; increasing this ratio increases the particle size for both surfactants. Both PIB and oleic acid appear to be good stabilizers for the particles in decalin. It was found that a significant amount of carbon was present in the particles, which were determined to consist of an amorphous $Fe_{0.75}C_{0.25}$ alloy. Particle sizes, measured with various techniques, correspond reasonably well with each other. Oleic-acid-coated particles are less polydisperse and have a more spherical shape than PIB-coated colloids. However, PIB-coated particles can be synthesized in a larger size range, due to the possibility to grow them from smaller particles. Iron concentrations are almost equal to the maximum theoretical value for the PIB-coated particles, whereas for dispersions of oleic-acid-coated particles free unconverted $Fe(CO)_5$ still seems to be present. Dispersions of smaller particles consist of single colloids, but dispersions of larger particles contain dynamic aggregates. Upon exposure to air, dispersions become unstable and a passivating oxide layer is formed on the particle surface, presumably consisting of a disordered nonmagnetic iron oxide. Particle sizes increase due to oxidation; the density of the oxide is smaller than of iron. Smaller particles oxidize more rapidly than larger ones. Particles do not oxidize completely; even after several months an iron core is still present, as was found from various techniques (except for very small particles A). If handled under nitrogen atmosphere iron dispersions, containing relatively monodisperse colloids, of which the particle size and thickness of the surfactant layer can be controlled over a broad range, are promising ferrofluids for studying the physical behavior of dipolar fluids. An interesting aspect is the dipolar structure formation in dispersions of larger particles in comparison

to sufficiently small particles, which are expected to remain dispersed as single colloids. This investigation is presented in [14–17].

Acknowledgments

Igor Dolbnya, Wim Bras, Dirk Detollenaere and Ruud van Tol from the DUBBLE beamline at the European Synchrotron Radiation Facility (ESRF) and Mohamed Ramzi from Rhodia Recherche (Aubervilliers, France) are thanked for their help with the SAXS measurements. Andrei Petukhov is thanked for valuable discussions. Maarten Terlou is thanked for assistance with analysis of the TEM micrographs. The infrared measurements were performed by Joop van der Maas. The XRD spectra were measured by Marjan Versluijs-Helder. Anton Goossens, Adri van der Kraan, Menno Crajé, Peter Paulus and Kees Flipse are thanked for the Mössbauer measurements and valuable discussions. Menno Crajé is thanked for carefully reading the manuscript. Financial support was granted by the Dutch Technology Foundation (STW) with financial aid from the Council for Chemical Science of the Netherlands Organization for Scientific Research (CW/NWO).

References

[1] S.S. Papell, in: U.S. Patent, vol. 3, 1965, p. 215.
[2] R.E. Rosensweig, Ferrohydrodynamics, Cambridge Univ. Press, Cambridge, 1985.
[3] B. Berkovski, V. Bashtovoy, Magnetic Fluids and Applications Handbook, Begel House, New York, 1996.
[4] G.A. van Ewijk, G.J. Vroege, B.W.M. Kuipers, Langmuir 18 (2002) 382.
[5] P.I.C. Teixeira, J.M. Tavares, M.M. Telo da Gama, J. Phys. Condens. Matter 12 (2000) R411.
[6] R. Massart, IEEE Trans. Magn. MAG-17 (1981) 1247.
[7] S. Sun, H. Zeng, J. Am. Chem. Soc. 124 (2002) 8204.
[8] D. Jiles, Introduction to Magnetism and Magnetic Materials, Chapman & Hall, London, 1995.
[9] S. Gangopadhyay, G.C. Hadjipanayis, B. Dale, C.M. Sorensen, K.J. Klabunde, V. Papaefthymiou, A. Kostikas, Phys. Rev. B 45 (1992) 9778.
[10] K.S. Suslick, F. Mingming, T. Hyeon, J. Am. Chem. Soc. 118 (1996) 11960.
[11] C.H. Griffiths, M.P. O'Horo, T.W. Smith, J. Appl. Phys. 50 (1979) 7108.
[12] T.W. Smith, D. Wychick, J. Phys. Chem. 84 (1980) 1621.
[13] C. Pathmamanoharan, N.L. Zuiverloon, A.P. Philipse, Prog. Colloid Polym. Sci. 115 (2000) 141.
[14] K. Butter, P.H. Bomans, P.M. Frederik, G.J. Vroege, A.P. Philipse, Nature Mater. 2 (2003) 88.
[15] K. Butter, P.H. Bomans, P.M. Frederik, G.J. Vroege, A.P. Philipse, J. Phys. Condens. Matter 15 (2003) S1451.
[16] B.H. Erné, K. Butter, B.W.M. Kuipers, G.J. Vroege, Langmuir 19 (2003) 8218.
[17] K. Butter, Iron(Oxide) Ferrofluids: Synthesis, Structure and Catalysis, Thesis, Utrecht University, 2003, ch. 4.
[18] B. De Hek, A. Vrij, J. Colloid Interface Sci. 79 (1981).
[19] O. Glatter, O. Kratky (Eds.), Small Angle X-ray Scattering, Academic Press, London, 1982.
[20] J.K.G. Dhont, An Introduction to Dynamics of Colloids, Elsevier, Amsterdam, 1996.
[21] L. Motte, F. Billoudet, P. Pileni, J. Phys. Chem. 99 (1995) 16425.
[22] C.G. de Kruif, W.J. Briels, R.P. May, Langmuir 4 (1988) 668.
[23] A.V. Petukhov, personal communication.
[24] J.K. Percus, G.J. Yevick, Phys. Rev. 110 (1958) 1.
[25] E. Thiele, J. Chem. Phys. 39 (1963) 474.
[26] S. Wertheim, Phys. Rev. Lett. 10 (1963) 321.
[27] P. van Beurten, A. Vrij, J. Chem. Phys. 74 (1981) 2744.
[28] A. Vrij, J. Chem. Phys. 71 (1979) 3267.
[29] R.J. Baxter, J. Chem. Phys. 52 (1970) 4559.
[30] K. Butter, A. Wiedenmann, A. Hoell, A.V. Petukhov, G.J. Vroege, J. Appl. Cryst. 37 (2004) 847.
[31] CRC Atlas of Spectral Data and Physical Constants for Organic Compounds, CRC Press, Cleveland, OH, 1973.
[32] Powder Diffraction File 2000, card 190629 ed., Joint Committee on Powder Diffraction Standards, Swarthmore, PA.
[33] A. Goossens, L.J. de Jongh, K. Butter, A.P. Philipse, M.W.J. Craje, A.M. van der Kraan, Hyperfine Interact. 141/142 (2002) 381.
[34] C. Pathmamanoharan, A.P. Philipse, J. Colloid Interface Sci. 205 (1998) 340.
[35] M.W.J. Crajé, personal communication.
[36] M. Hanson, C. Johansson, M.S. Pedersen, S. Morup, J. Phys. Condens. Matter 7 (1995) 9269.
[37] E. Bauer-Grosse, G. Le Caër, Philos. Mag. B 56 (1987) 485.